

2493 **Chapter 10**
2494 **Strong Focusing Synchrotron**

2495 **Abstract** This Chapter introduces the strong focusing synchrotron, alternating gra-
2496 dient (AG) and separated focusing, and the theoretical material needed for the simula-
2497 tion exercises. It begins with a brief reminder of the historical context, and continues
2498 with beam optics, chromaticity, and acceleration. It relies on basic charged particle
2499 optics and acceleration concepts introduced in the previous Chapters, and further
2500 addresses the following aspects:

- 2501 - resonances and resonant extraction,
- 2502 - stochastic energy loss by synchrotron radiation.

2503 The simulation of a strong focusing synchrotron requires just two, possibly three,
2504 optical elements from zgoubi library: DIPOLE, BEND, or MULTIPOL to sim-
2505 ulate (possibly combined function) dipoles, DRIFT to simulate straight sections,
2506 and MULTIPOL to simulate lenses (which can be otherwise simulated using
2507 QUADRUPO, SEXTUPOL, OCTUPOLE, etc.). A fourth element, CAVITE, is re-
2508 quired for acceleration. Particle monitoring requires keywords introduced in the pre-
2509 vious Chapters, including FAISCEAU, FAISTORE, possibly PICKUPS, and some
2510 others. Spin motion computation and monitoring resort to SPNTRK, SPNPRT, FAI-
2511 STORE. Optics matching and optimization use FIT[2]. INCLUDE is used, mostly
2512 here in order to shorten the input data files. SYSTEM is used to, mostly, resort to
2513 gnuplot so as to end simulaitions with some specific graphs obtained by reading
2514 data from output files such as zgoubi.fai (resulting from the use of FAISTORE),
2515 zgoubi.plt (resulting from IL=2), or other zgoubi.*.out files resulting from a PRINT
2516 command.

2517 **Notations used in the Text**

$B; \mathbf{B}, B_{x,y,s}$	field value; field vector, its components in the moving frame
$B\rho = p/q; B\rho_0$	particle rigidity; reference rigidity
$C; C_0$	orbit length, $C = 2\pi R + \left[\begin{array}{l} \text{straight} \\ \text{sections} \end{array} \right]$; reference, $C_0 = C(p = p_0)$
E	particle energy
EFB	Effective Field Boundary
$f_{\text{rev}}, f_{\text{rf}} = f_{\text{rev}}$	revolution and accelerating voltage frequencies
G	gyromagnetic anomaly, $G = 1.792847$ for proton
$G; K = G/B\rho$	quadrupole gradient; focusing strength
$m; m_0; M$	mass, $m = \gamma m_0$; rest mass; in units of MeV/c ²
$\mathbf{p}; p; p_0$	momentum vector; its modulus; reference
P_i, P_f	beam polarization, initial, final
q	particle charge
r, R	orbital radius ; average radius, $R = C/2\pi$
s	path variable
v	particle velocity
$V(t); \hat{V}$	oscillating voltage; its peak value
$x, x', y, y', l, \frac{dp}{p}$	horizontal, vertical, longitudinal coordinates in moving frame

2518

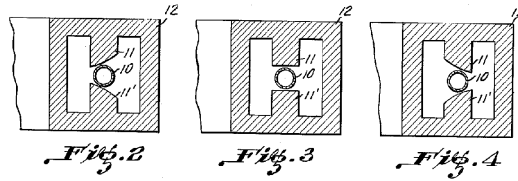
α	momentum compaction
α	trajectory angle
$\beta = v/c; \beta_0; \beta_s$	normalized particle velocity; reference; synchronous
β_u	betatron functions ($u : x, y, Y, Z$)
$\gamma = E/m_0$	Lorentz relativistic factor
δp	momentum offset or Dirac distribution
Δp	momentum offset
ε	wedge angle
ε_u	Courant-Snyder invariant ($u : x, r, y, l, Y, Z, s, \text{etc.}$)
ε_R	strength of a depolarizing resonance
μ_u	betatron phase advance, $\mu_u = \int_{\text{period}} ds/\beta_u(s)$ ($u : x, y, Y, Z$)
ν_u	wave numbers, horizontal, vertical, synchrotron ($u : x, y, Y, Z, l$)
ρ, ρ_0	curvature radius; reference
σ	beam matrix
$\phi; \phi_s$	particle phase at voltage gap; synchronous phase
ϕ_u	betatron phase advance, $\phi_u = \int ds/\beta_u$ ($u : x, y, Y, \text{or } Z$)
φ	spin angle to the vertical axis

2519 **10.1 Introduction**

2520 In the very manner that the 1930s-1940s cyclotron, betatron, microtron, weak fo-
 2521 cusing synchrotron, still in use today, have since essentially not changed in their

2522 concepts, design principles, magnet gap profile, today's gap profile, yoke and cur-
 2523 rent coil geometry of combined function alternating-gradient (AG) dipoles remain
 essentially as patented in 1950 (Fig. 10.1) [1].

Fig. 10.1 Bending magnet pole profiles for a focussing system for ions and electrons [1]. Assuming curvature center to the left, the right (respectively left) profile is defocusing (resp. focusing), the middle profile has zero index



2524 In 1952, in the context of studies relative to the Cosmotron, strong focusing was
 2525 devised at the Brookhaven National Laboratory (BNL): “*Strong focusing forces re-*
 2526 *sult from the alternation of large positive and negative n-values in successive sectors*
 2527 *of the magnetic guide field in a synchrotron. This sequence of alternately conver-*
 2528 *ing and diverging magnetic lenses [...] leads to significant reductions in oscillation*
 2529 *amplitude*” [2]. It led to the construction of the first two high-energy proton AG
 2530 synchrotrons, in the 30 GeV range, in the late 1950s: the proton-synchrotron (PS)
 2531 at CERN, and the AGS at BNL, major pieces 60 years later still, of the respective
 2532 injection chains of the two largest colliders in operation, the LHC and RHIC. Early
 2533 works at BNL provided theoretical formalism, still at work today, for the analysis of
 2534 beam dynamics in synchrotrons [3].

2536 The optical principle behind the AG concept is that a doublet of focusing and
 2537 defocusing lenses with proper strengths results in a, possibly quite strong, very short
 2538 focal distance, converging system. The dramatic effect of strong-index AG on trans-
 2539 verse beam size allows small dipole gaps, thus small magnets: from lowest energies
 2540 (medical synchrotrons in the 100 MeV range for instance) to the highest ones (par-
 2541 ticle physics and nuclear physics colliders, hundreds of GeV to multi-TeV range),
 2542 beams are essentially confined in a centimeter scale transverse space, making a syn-
 2543 chrotron a string of dipole magnets containing beam in a ring vacuum pipe of cm to
 2544 10 cm diameter; the size of the ring is essentially determined by its circumference,
 2545 proportional to the magnetic rigidity. This revolutionized the race to high energies,
 2546 from an upper 10 GeV about of the prior weak focusing synchrotrons and their huge
 2547 magnets, to today's 7 TeV at the LHC with magnets transverse size in the meter range,
 2548 and with further plans for 100 TeV rings [5]. It fostered as well the development of
 2549 high energy synchrotron light sources around the world, with electron beam energies
 2550 up to 8 GeV.

2551 The original AG dipole design (that of the PS and AGS rings), whereby gradient
 2552 dipoles combine beam guiding and beam focusing, has the benefit of compactness.
 2553 It is still prized today and resorted to, for instance in hadrontherapy applications
 2554 (Fig. 10.3); light source lattice vertical focusing [7], etc. Separated function AG
 2555 focusing, whereby beam guiding is ensured by uniform field dipoles while focusing
 2556 is ensured separately by quadrupoles, followed from the development of the latter

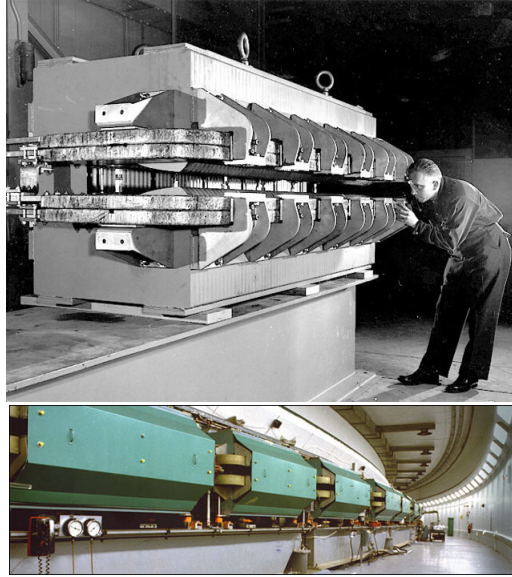


Fig. 10.2 Top: the AGS combined function main magnet - one of 240 steering the beam around the ring, bottom: the 809 m circumference AGS synchrotron [4]. The hyperbolic profile poles are visible on the top photo, partly hidden by the field coils

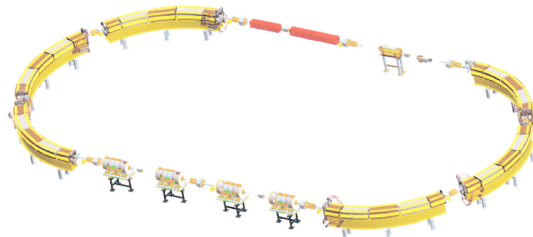


Fig. 10.3 The ion rapid cycling medical synchrotron (iRCMS) [6], an RCS aimed at providing ion beams for the treatment of cancer tumours

2557 (Fig.10.4), a spin-off of the strong index technology [8]. Separated function optics
 2558 has the merit of flexibility, allowing modular functions in complex rings such as
 2559 bending-free dispersion suppression sections, low-beta collision or insertion device
 2560 sections, long straights, etc. Low-emittance, high-brightness light source lattices
 2561 have complicated focusing further, by introducing longitudinal field gradient bending
 2562 systems, aimed at minimizing the chromatic invariant [9].

2563 Due to the necessary ramping of the field in order to maintain a constant orbit,
 2564 synchrotrons accelerators are pulsed, some storage rings species are pulsed as well,
 2565 high energy colliders in particular to bring beams to highest store energy. The accel-
 2566 eration is cycled and the accelerating voltage frequency as well in ion accelerators,
 2567 from injection to top energy. If the ramping uses a constant electromotive force, then
 2568 (Eq. 9.3)

$$B(t) \approx \frac{t}{\tau} \quad (10.1)$$

Fig. 10.4 A quadrupole magnet at LBL in 1957, used for beam lines at the 184-inch cyclotron. An early specimen here, obviously, being a spin-off of the early 1950s concept of strong focusing [10]



2569 $\dot{B} = dB/dt$ does not exceed a few Tesla/second, thus the repetition rate of the
 2570 acceleration cycle is of the order of a Hertz. If instead the magnet winding is part of
 2571 a resonant circuit then the field oscillate,

$$B(t) = B_0 + \frac{\hat{B}}{2}(1 - \cos \omega t) \quad (10.2)$$

2572 so that, in the interval of half a voltage repetition period (*i.e.*, $t : 0 \rightarrow \pi/\omega$) the
 2573 field increases from an injection threshold value to a maximum value at highest
 2574 rigidity, $B(t) : B_0 \rightarrow B_0 + \hat{B}$. The latter determines the highest achievable energy:
 2575 $\hat{E} = pc/\beta = q\hat{B}pc/\beta$. The repetition rate with resonant magnet cycling can reach
 2576 a few tens of Hertz, a species known as a rapid-cycling synchrotron (RCS). In both
 2577 cases anyway B imposes its law and the other quantities comprising the acceleration
 2578 cycle (RF frequency in particular) will follow B(t).

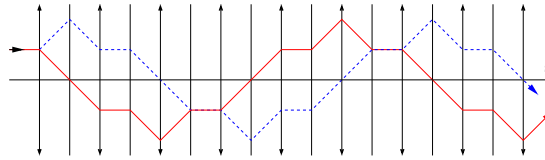
2579 Rapid cycling allows high intensity beams. Instances are the Cornell 12 GeV,
 2580 60 Hz, electron synchrotron, commissioned in 1967, today the injector of Cornell
 2581 5 GeV synchrotron light source (CHESS); Fermilab 8 GeV, 60 Hz, booster which
 2582 provides protons for the production of neutrino beams; the 30 GeV 500 kW beam J-
 2583 PARC facility in Japan. Rapid cycling is also considered in ion-therapy applications,
 2584 Fig. 10.3.

2585 10.2 Basic Concepts and Formulæ

2586 Alternating gradient focusing is sketched in Fig. 10.5.

2587 The focusing index value can be estimated from the fields met in these structures:
 2588 a maximum $B \sim 1$ Tesla in the dipole gap, and as well at pole tip in quadrupoles
 2589 ~ 10 cm off axis. The latter results in $\frac{\Delta B}{\Delta x} \sim 10$ T/m, the former in \sim meters to tens of
 2590 meters dipole curvature radius. All in all,

Fig. 10.5 Horizontally focusing lenses (field index $n \gg 0$, the solid red trajectory) are vertically defocusing ($n \ll 0$, the dashed blue trajectory), and vice versa. This imposes alternating gradients in order for a sequence to be globally focusing.



$$n = \frac{\rho}{B} \frac{\partial B}{\partial x} \sim \frac{10^{0-2} \text{ [m]}}{1 \text{ [T]}} \times 10 \text{ [T/m]} \sim 10^{1-3} \gg 1 \quad (10.3)$$

2591 much greater than in a weak focusing structure, characterized by $0 < n < 1$.

2592 10.2.1 Components of the Strong Focusing Optics

2593 Combined function (AG) optics

2594 This is, typically, the BNL AGS and CERN PS optics, using dipoles that ensure both
2595 beam guiding and focusing (Fig. 10.2). Separate quadrupole and multipole lenses
2596 have later been introduced in these lattices as they provide knobs for the adjustment
2597 of optical functions and parameters.

2598 AG optics is still at work in modern designs, as in the iRCMS whose six 60 deg
2599 arcs are comprised of a sequence of five focusing and defocusing combined function
2600 dipoles [6], Fig. 10.3.

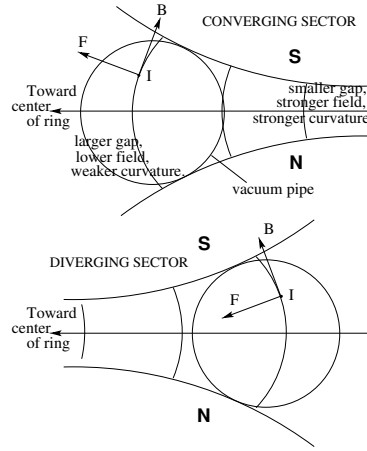
2601 *Field*

2602 Referring to the normal conducting magnet technology, an hyperbolic pole profile
2603 (Fig. 10.1): equipotential $V(x, y) = Axy$ (A a constant, typically $\sim 10 \text{ T/m}$, cf.
2604 Eq. 10.3), results in $B_y = \frac{\partial V}{\partial y} = Ax$, i.e. a radial field index $n = \frac{\rho}{B_y} \frac{\partial B}{\partial x} |_{y=0}$,
2605 responsible for the focusing; the pole profile opens up either inward (toward the
2606 center of curvature, a horizontally focusing dipole, vertically defocusing) or outward
2607 (a vertically focusing dipole, horizontally defocusing), Fig. 10.6.

2608 In a straight AG dipole a line of constant field is a straight line; an instance is
2609 the AGS main magnet (Fig. 10.2). Another instance is the Fermilab recycler arcs
2610 permanent magnet dipole, which includes quadrupole and sextupole components [11,
2611 12]. The modeling of the field can be derived from the Laplace potential $V(s, x, y)$,
2612 see below; the AGS on-line model uses that technique [13].

2613 In a bent AG dipole a line of constant field is an arc of a circle; the field guides
2614 the reference particle along the arc in the median plane. The mid-plane field can be
2615 expressed as

Fig. 10.6 Beam focusing in combined function dipoles. The center of curvature is to the left. The pole profile follows an equipotential $V = axy$. Top: the pole profile opens up towards the center of curvature \rightarrow the dipole is horizontally converging (vertically diverging: current I comes out of the page, force F results from field B). Bottom: pole profile closing toward the center of curvature \rightarrow the dipole is horizontally diverging, vertically converging



$$B_y(r, \theta) = \mathcal{G}(r, \theta) B_0 \left(1 + n \frac{r - r_0}{r_0} + n_2 \left(\frac{r - r_0}{r_0} \right)^2 + n_3 \left(\frac{r - r_0}{r_0} \right)^3 + \dots \right) \quad (10.4)$$

2616 with r_0 the eference radius. Higher order indices, sextupole n_2 , octupole n_3 , ...,
 2617 may be residual effects: fabrication tolerance, saturation, magnetic permeability,
 2618 deformation of yoke with years, ..., as in the AGS dipoles, or included by design.

2619 In a straight AG dipole a line of constant field is a straight line; an instance is
 2620 the AGS main magnet (Fig. 10.2). Another instance is the Fermilab recycler arcs
 2621 permanent magnet dipole, which includes quadrupole and sextupole components [11,
 2622 12]. The modeling of the field in a straight combined function dipole can be derived
 2623 from the scalar potential of Eq. 10.5.

2624 Separated function optics

2625 Main bends have zero index and ensure beam guiding. In smaller rings though,
 2626 bending may contribute horizontal focusing; wedge angles in addition may be intro-
 2627 duced and contribute some horizontal and vertical focusing/defocusing. Quadrupole
 2628 lenses, alternately focusing and defocusing, ensure the essential of the focusing.

2629 Higher order multipole lenses are used for the compensation of adverse effects:
 2630 coupling, aberrations, space charge, impedance, etc., and for beam manipulations:
 2631 coupling, resonant extraction, etc.

2632 The field in a multipole of order n ($n = 1, 2, 3, \dots$: dipole, quadrupole, sextupole,
 2633 ...) derives, via $\mathbf{B} = \mathbf{grad}V$, from the Laplace potential [14]

$$V_n = (n!)^2 \left\{ \sum_{q=0}^{\infty} (-)^q \alpha_{n,0}^{(2q)}(s) \frac{(x^2 + y^2)^q}{4^q q!(n+q)!} \right\} \left\{ \frac{x^{n-m} y^m}{m!(n-m)!} \sin m \frac{\pi}{2} \right\} \quad (10.5)$$

2634 wherein $\alpha_{n,0}^{(2q)} = d^{2q}\alpha_{n,0}/ds^{2q}$ accounts for the s -dependence of the field form
 2635 factor. Technologies for multipoles and combined multipoles include warm magnets
 2636 and pole profiling (Figs. 10.2, 10.4), permanent magnets [11, 15], superconducting
 2637 magnets and $\cos \theta$ windings as in RHIC and LHC colliders, and variants.

2638 In a hard-edge model the left sum in Eq. 10.5 is reduce to the $q = 0$ term, with
 2639 the following outcomes.

2640 *Quadrupole*

The equipotential (the pole profile) is an hyperbola: $Gxy = \text{constant}$, in an upright
 quadrupole (left), $G(x^2 - y^2) = \text{constant}$ in a $\pi/4$ skewed quadrupole (right); the
 resulting field writes

$$\begin{aligned}
 B_x &= \frac{\partial V}{\partial x} = Gy \\
 B_y &= \frac{\partial V}{\partial y} = Gx
 \end{aligned}
 \quad
 \begin{array}{c}
 \text{Left: Upright quadrupole} \\
 \text{Right: } \pi/4 \text{ skewed quadrupole}
 \end{array}
 \quad
 \begin{aligned}
 B_x &= Gx \\
 B_y &= -Gy
 \end{aligned}$$

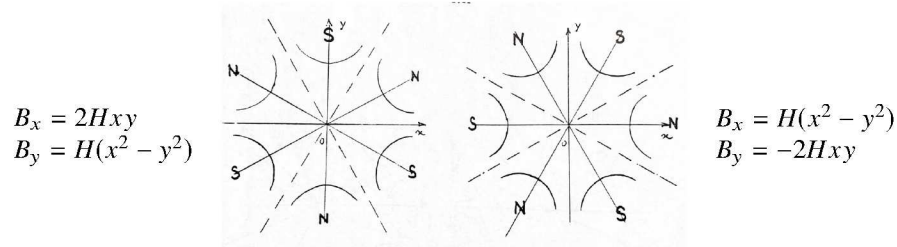
Upright quadrupoles are used for focusing, skew quadrupoles are used to compensate,
 or introduce, transverse coupling. Their focusing strength

$$K = \frac{1}{L} \frac{\int G(s) ds}{p/q}$$

2641 is momentum-dependent.

2642 *Sextupole*

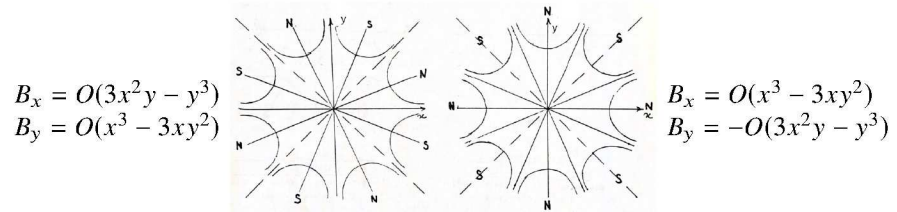
The equipotential satisfies $H(3x^2y - y^3) = \text{constant}$ in an upright sextupole (left),
 $H(x^3 - 3xy^2) = \text{constant}$ in a $\pi/6$ skewed sextupole (right), with resulting field



2643 Upright sextupoles introduce a vertical field component $B_y \propto x^2$, they are used
 2644 to correct optical aberrations, to modify the momentum dependence of the wave
 2645 numbers ν_x , ν_y , and in beam manipulations such as resonante extraction. Skew
 2646 sextupoles introduce a radial field component $B_x \propto y^2$, they are used to correct
 2647 optical aberrations.

2648 *Octupole*

The equipotential pole profile satisfies $O(x^3y - xy^3) = \text{constant}$ in an upright octupole
 (left), $O(x^4 - 6x^2y^2 + y^4) = \text{constant}$ in a $\pi/8$ skewed octupole (right), yielding the
 field



2649 Upright octupoles are used to introduce a vertical field componnet $B_y \propto x^3$; skew
 2650 octupoles introduce a vertical field component $B_y \propto y^3$ Octupoles are used to correct
 2651 aberrations, or to modify the amplitude dependence of wave numbers.

2652 **10.2.2 Transverse motion**

2653 The transverse motion of a particle in the periodic lattice of a ring acceleratiior
 2654 satisfies Hill's equations

$$\frac{d^2x}{ds^2} + K_x(s)x = \frac{1}{\rho_0} \frac{\Delta p}{p_0}, \quad \frac{d^2y}{ds^2} + K_y(s)y = 0 \quad (10.6)$$

2655 wherein $K_x(s)$, $K_y(s)$ have the periodicity of the lattice, and depend locally on the
2656 nature of the optical elements:

$$\begin{aligned} \text{-- dipole :} & \quad \begin{cases} K_x = \frac{1-n}{\rho_0^2} \\ K_y = \frac{n}{\rho_0^2} \end{cases} \quad (n = -\frac{\rho_0}{B_0} \frac{\partial B_y}{\partial x}) \\ \text{-- a wedge at } s = s_0 : & \quad \begin{cases} K_x \\ K_y \end{cases} = \pm \frac{\tan \varepsilon}{\rho_0} \delta(s - s_0) \quad (\varepsilon \leq 0 : \begin{matrix} \text{focusing} \\ \text{defocusing} \end{matrix}); \quad \frac{1}{\rho_0} = 0 \\ \text{-- quadrupole} & \quad (\text{gradient } G = \frac{\text{field at pole tip}}{\text{radius at pole tip}}) : \quad K_x = \frac{\pm G}{B\rho}; \quad \frac{1}{\rho_0} = 0 \\ \text{-- drift space :} & \quad K_x = K_y = 0; \quad \frac{1}{\rho_0} = 0 \end{aligned} \quad (10.7)$$

2657 By contrast with the single index ($0 < n < 1$) betatron and weak focusing
2658 technologies, strong focusing with its independent focusing ($G > 0$) and defocusing
2659 ($G < 0$) families allows separate adjustment of the horizontal and vertical focusing
2660 strengths, and wave numbers as a consequence.

2661 The on-momentum ($p = p_0$) closed orbit coincides with the reference axis of
2662 the optical structure. The betatron motion for an on-momentum particle, *i.e.* the
2663 excursion x , y around the closed orbit, satisfies Eq. 10.6 with $\Delta p = 0$. Solving the
2664 latter (see Sect. 9.2) requires introducing two independent solutions $u_{1,2}(s)$ (Eq. 9.12),
2665 the linear combination of which yields the pseudo harmonic motion (Eq. 9.15)

$$\begin{cases} u(s) = \sqrt{\beta(s)\varepsilon/\pi} \cos\left(\int \frac{ds}{\beta(s)} + \varphi\right) \\ u'(s) = -\sqrt{\frac{\varepsilon/\pi}{\beta(s)}} \sin\left(\int \frac{ds}{\beta(s)} + \varphi\right) + \alpha(s) \cos\left(\int \frac{ds}{\beta(s)} + \varphi\right) \end{cases} \quad (10.8)$$

2666 The motion satisfies the Courant-Snyder invariant, namely (Fig. 9.10)

$$\gamma_u(s)u^2 + 2\alpha_u(s)uu' + \beta_u(s)u'^2 = \frac{\varepsilon_u}{\pi} \quad (10.9)$$

2667 The form and the orientation of this phase space ellipse change along the period, its
2668 surface is constant.

2669 Beam envelopes are given by the extrema,

$$\hat{x}_{\text{env}}(s) = \pm \sqrt{\beta_x(s) \frac{\varepsilon_x}{\pi}}, \quad \hat{y}_{\text{env}}(s) = \pm \sqrt{\beta_y(s) \frac{\varepsilon_y}{\pi}} \quad (10.10)$$

2670 *Phase space motion*2671 Write the two independent solutions $u_{1,2}(s)$ (Eq. 9.12) under the form

$$u_1(s) = \underbrace{F(s)}_{S\text{-periodic}} \times \underbrace{e^{i\mu\frac{s}{S}}}_{\frac{2\pi S}{\mu}\text{-periodic}} \quad \text{and} \quad u_2(s) = u_1^*(s) = F^*(s) e^{-i\mu\frac{s}{S}} \quad (10.11)$$

2672 wherein $F(s) = \sqrt{\beta(s)} e^{i\left(\int_0^s \frac{ds}{\beta(s)} - \mu\frac{s}{S}\right)}$. Introduce $\psi(s) = \int_0^s \frac{ds}{\beta(s)} - \mu\frac{s}{S}$ so that2673 $F(s) = \sqrt{\beta(s)} e^{i\psi(s)}$, Eq. 10.8 thus takes the form

$$\left\{ \begin{array}{l} u(s) = \underbrace{\sqrt{\beta(s)\varepsilon/\pi}}_{S\text{-periodic}} \underbrace{\cos\left[v\frac{s}{R} + \underbrace{\psi(s) + \varphi}_{S\text{-per.}}\right]}_{\frac{2\pi S}{\mu}\text{-periodic}} \\ u'(s) = -\sqrt{\frac{\varepsilon/\pi}{\beta(s)}} \sin\left[v\frac{s}{R} + \psi(s) + \varphi\right] + \alpha(s) \cos\left[v\frac{s}{R} + \psi(s) + \varphi\right] \end{array} \right. \quad (10.12)$$

2674 wherein $\nu = \frac{N\mu}{2\pi}$. Thus, as $\beta(s)$ and $\psi(s)$ are S -periodic functions, the turn-by-turn
 2675 motion observed at a given azimuth s (i.e., $u(s)$, $u(s+S)$, $u(s+2S)$, ...) is sinusoidal
 2676 with frequency $\nu = N\mu/2\pi$. Successive particle positions ($u(s)$, $u'(s)$) in phase space
 2677 lie on the Courant-Snyder invariant (Eq. 10.9).

2678 The wave numbers ν_x and ν_y can be adjusted independently in a separated function
 2679 lattice, by means of two independent quadrupole families. The working point (ν_x, ν_y)
 2680 fully characterizes the first order optical setting of the ring.

2681 *Off-momentum motion*

2682 The motion of an off-momentum particle satisfies the inhomogeneous Hill's hori-
 2683 zontal differential Eq. 10.6. The chromatic closed orbit

$$x_{\text{ch}}(s) = D_x(s) \frac{\delta p}{p} \quad (10.13)$$

2684 is a particular solution of the equation, its periodicity is that of the cell.

2685 By contrast with the weak focusing configuration, where the on-momentum closed
 2686 orbit and chromatic closed orbits are parallel (Eq. 9.26: $D_x = \text{constant}$, independent of
 2687 s), chromatic closed orbits in a strong focusing optical structure are distorted, their
 2688 excursion depends on the distribution along the cell of (i) the dispersive elements
 2689 which are the dipoles, and (ii) the focusing.

2690 The horizontal motion of an off-momentum particle is a superposition of the par-
 2691 ticular solution (Eq. 10.13) and of the betatron motion, solution of the homogeneous
 2692 Hill's equation (Eq. 9.22 with $\delta p/p = 0$), namely

$$x(s) = x_{\beta}(s) + x_{\text{ch}}(s) = \sqrt{\beta_x(s) \frac{\varepsilon_x}{\pi}} \cos\left(\int \frac{ds}{\beta_x} + \varphi\right) + D_x(s) \frac{\Delta p}{p_0} \quad (10.14)$$

2693 whereas the vertical motion is unchanged (Eq. 10.12 taken for $u(s) \equiv y(s)$).

2694 10.2.3 Resonances. Resonant Extraction

2695 Consider the excitation of transverse beam motion by a generator of frequency Ω
 2696 located at some azimuth along the ring [16]. The action of the excitation $S \times \sin \Omega t$
 2697 on the oscillating motion $u(t)$ can be written under the form

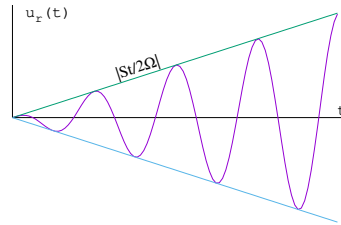
$$\frac{d^2 u}{dt^2} + \omega^2 u = S \sin \Omega t \quad (10.15)$$

2698 The betatron motion is assumed harmonic for simplicity, case for instance of weak
 2699 focusing. Take S constant, the solution (superposition of the solution of the ho-
 2700 mogeneous differential equation and of a particular solution of the inhomogeneous
 2701 differential equation) writes

$$u(t) = U \cos(\omega t + \varphi) + \frac{S}{\omega^2 - \Omega^2} \sin \Omega t \quad (10.16)$$

If betatron motion and excitation are in synchronism, *i.e.* on the resonance, $\omega = \Omega$,
 a particular solution of Eq. 10.15 is

$$u_r(t) = -\frac{S t}{2\Omega} \cos \Omega t$$



2702 the amplitude of the oscillatory motion grows rapidly with time, at a rate $|St/2\Omega|$.

Assume S periodic instead, take its Fourier expansion $S(t) = \sum_{p=0}^{\infty} a_p \cos(p\omega' t + \varphi_p)$, the equation of motion thus writes

$$\frac{d^2 u}{dt^2} + \omega^2 u = \sum_{p=0}^{\infty} a_p \cos(p\omega' t + \varphi_p) \sin \Omega t =$$

$$\sum_{p=0}^{\infty} \frac{a_p}{2} \left[\sin[(\Omega - p\omega')t + \varphi_p] + \sin[(\Omega + p\omega')t + \varphi_p] \right]$$

2703 Resonance may occur at oscillator frequencies $\omega = \Omega \pm p\omega'$, their strength depends
 2704 on the amplitude a_p of the excitation harmonics. If the generator is located at one
 2705 point in the ring, it excites all harmonics.

2706 *Sextupole and octupole resonances*

2707 The horizontal motion in the presence of a sextupole component $(B_y(\theta)|_{y=0} = S(\theta)x^2$,
 2708 see *Sextupole*, above) as part of the ring optical lattice satisfies

$$\frac{d^2x}{d\theta^2} + \nu_x^2 x = S(\theta)x^2 \quad (10.17)$$

Assume weak perturbation of the motion, so that $x(\theta) \approx \hat{x} \cos(\nu_x \theta + \varphi)$; the perturbation $S(\theta)$ is 2π -periodic thus substitute its Fourier series expansion $S(\theta) = \sum_{p=0}^{\infty} a_p \cos(p\omega'\theta + \varphi_p)$ in the differential equation; develop to get

$$\frac{d^2x}{d\theta^2} + \nu_x^2 x = \frac{\hat{x}^2}{2} \sum_{p=0}^{\infty} a_p \left[\cos(p\theta + \varphi_p) + \cos[(p - 2\nu_x)\theta + \varphi_p - 2\varphi] + \cos[(p + 2\nu_x)\theta + \varphi_p + 2\varphi] \right]$$

Thus resonance may occur at betatron frequency families $\nu_x = \pm p$, $\nu_x = \pm(p - 2\nu_x)$, and $\nu_x = \pm(p + 2\nu_x)$, *i.e.*,

$$\begin{cases} \nu_x = \text{integer} \\ 3\nu_x = \text{integer} \end{cases}$$

2709 In the case of a single sextupole in the ring, all the harmonics p are excited with the
 2710 same amplitude a_p .

An octupole perturbation introduces a field component $B_y(\theta)|_{y=0} = O(\theta)x^3$ (see *Octupole*, above) in the optical lattice. In a similar way, assume weak perturbation so that $x(\theta) \approx \hat{x} \cos(\nu_x \theta + \varphi)$; to $O(\theta)$ substitute its Fourier expansion; this yields

$$\begin{cases} \nu_x = \text{integer} \\ 2\nu_x = \text{integer} \\ 4\nu_x = \text{integer} \end{cases}$$

Resonances in a general manner occur at betatron frequencies satisfying

$$m\nu_x + n\nu_y = \text{integer}$$

with the property that

$$\frac{\varepsilon_x}{m} - \frac{\varepsilon_y}{n} = \text{constant}, \quad \text{an invariant of the motion}$$

2711 with the following consequences:

2712 - if m and n have opposite signs the resonance causes energy exchange between the
 2713 horizontal and vertical motions: $\frac{\varepsilon_x}{|m|} + \frac{\varepsilon_y}{|n|} = \text{constant}$, an increase of ε_x correlates
 2714 with a decrease of ε_y and vice-versa; in the presence of linear coupling for instance,
 2715 $\nu_x - \nu_y = \text{integer}$, $\varepsilon_x + \varepsilon_y = \text{constant}$; an increase in motion amplitude anyway may
 2716 cause particle loss, an issue in cyclotrons with the Walkinshaw resonance $\nu_x = 2\nu_y$
 2717 which causes vertical beam loss upon increase of ε_y ;

2718 - if m and n have the same sign the resonance induces motion instability: $\frac{\varepsilon_x}{m} - \frac{\varepsilon_y}{n} =$
 2719 constant, ε_x and ε_y may both increase with no limit.

2720 Resonant Extraction

2721 10.2.4 Synchrotron Motion

2722 Particle motion in the longitudinal phase space (phase, momentum) is determined
 2723 by the lattice and by the acceleration parameters. The synchrotron acceleration
 2724 technique has been discussed in Sect. 9.2.2, outcomes are leaned on, here.

2725 Acceleration parameters include RF voltage \hat{V} , frequency $f_{\text{rf}} = \omega_{\text{rf}}/2\pi$, *****
 2726 Transition γ_{tr} is a property of the lattice and determines the synchronous phase
 2727 region, $[0, \pi/2]$ or $[\pi/2, \pi]$.

Synchrotron angular frequency

$$\Omega_s = (\omega_{\text{rev}}^2 |\eta| h_{\text{RF}} e \hat{V} \cos \phi_s / 2\pi E_s)^{1/2}$$

2728 with $\eta = 1/\gamma^2 - \alpha$ the phase slip factor (Eq. 9.33), h_{RF} the RF harmonic, $\omega_{\text{rev}} =$
 2729 $2\pi/T_{\text{rev}}$ the revolution angular frequency, \hat{V} the RF peak voltage, ϕ_s the synchronous
 2730 phase.

2731 The bucket height, “momentum acceptance”, satisfies

$$\pm \frac{\Delta p}{p} = \pm \frac{1}{\beta} \sqrt{\frac{q \hat{V}}{\pi h \eta E_s} [-(\pi - 2\phi_s) \sin \phi_s + 2 \cos \phi_s]} \quad (10.18)$$

$$\alpha = \frac{\Delta C}{C} \Big/ \frac{\Delta p}{p_0} \equiv \frac{\Delta R}{R} \Big/ \frac{\Delta p}{p_0} \quad (10.19)$$

2732 The maximum extent in phase for small amplitude oscillations satisfies

$$\pm \Delta \varphi_{\text{max}} = \frac{h \eta E_s}{p_s R_s \Omega_s} \times \max \left(\frac{\Delta E}{E_s} \right) \quad (10.20)$$

2733 ***** separatrix *****

2734 The motion of a particle with energy offset $\delta E = E - E_s$ satisfies the longitudinal
2735 invariants

$$\epsilon_l = \frac{\alpha E_s}{2\Omega_s} \left[\left(\frac{\delta E}{E_s} \right)^2 + \frac{1}{\Omega_s^2} \left(\frac{d \delta E}{dt} \right)^2 \right] \quad (10.21)$$

2736

$$(\widehat{\delta E})^2 = (\delta E)^2 + \frac{1}{\Omega_s^2} \left(\frac{d\delta E}{dt} \right)^2 \quad (10.22)$$

2737 Introducing the squared *rms* relative synchrotron amplitude $\sigma_{\delta E/E}^2 \equiv (\widehat{\delta E}/E_s)^2$ this
2738 yields in addition

$$\epsilon_l = \frac{\alpha E_s}{2\Omega_s} \sigma_{\delta E/E}^2 \quad (10.23)$$

2739 10.2.5 Radiative Energy Loss

2740 check what was said in betatron chapter ...

2741 A particle of rest mass m_0 and charge e travelling in a magnetic field is subject
2742 to stochastic photon emission, which causes energy loss [19]. The phenomenon
2743 involves two random processes:

2744 - the probability of photon emission over a trajectory arc δs , a Poisson law,

$$p(k) = \frac{\Lambda^k}{k!} e^{-\Lambda} \quad \text{with} \quad \Lambda = \langle k \rangle = \langle k^2 \rangle \quad (10.24)$$

2745 wherein k is the number of photons emitted over δs , $\Lambda = \frac{5e r_0}{2\hbar\sqrt{3}} B \rho \frac{\delta s}{\rho}$ is its average
2746 value, $r_0 = e^2 / 4\pi\epsilon_0 m_0 c^2$ is the classical radius of the particle, $\epsilon_0 = 1 / 36\pi 10^9$, \hbar is
2747 the Plank constant,

2748 - the energy ϵ of the photon(s), following the probability law

$$\mathcal{P} \left(\frac{\epsilon}{\epsilon_c} \right) = \frac{3}{5\pi} \int_0^{\epsilon/\epsilon_c} \frac{d\epsilon}{\epsilon_c} \int_{\epsilon/\epsilon_c}^{\infty} K_{5/3}(x) dx \quad (10.25)$$

2749 with $K_{5/3}$ the modified Bessel function, $\gamma = E/E_0$ with $E_0 = m_0 c^2$ the rest energy,
2750 and ϵ_c the critical energy of the radiation,

$$\epsilon_c = \frac{3\hbar\gamma^3 c}{2\rho} \quad (10.26)$$

2751 The average energy loss over δs is, assuming ultra-relativistic particles: $\beta = v/c \approx 1$,

$$\delta E = \frac{2}{3} r_0 E_0 \gamma^4 \frac{\delta s}{\rho^2} = \frac{2}{3} r_0 e c \gamma^3 B \frac{\delta s}{\rho} \approx \underbrace{1.88 \cdot 10^{-15} \gamma^3 \frac{\delta s}{\rho^2}}_{\text{for electrons}} \quad (10.27)$$

2752 The energy spread resulting from the stochastic emission is

$$\sigma_{\delta E/E} = \frac{\sqrt{110\sqrt{3}\hbar c / \pi\epsilon_0}}{24E_0/e} \gamma^{5/2} \frac{\sqrt{\delta s}}{\rho^{3/2}} \approx \underbrace{3.80 \cdot 10^{-14}}_{\text{for electrons}} \gamma^{5/2} \frac{\sqrt{\delta s}}{\rho} \quad (10.28)$$

2753 In a storage ring the RF system restores on average the energy lost by SR. Usefull
2754 formulas are given in Tab. 10.1, in particular, assuming a flat ring the partition
2755 of energy between radial and longitudinal motions is determined by the partition
2756 numbers

$$J_x = 1 - \mathcal{D}, \quad J_y = 1, \quad J_l = 2 + \mathcal{D}, \quad \text{with } \mathcal{D} = \frac{\overline{D_x(1-2n)/\rho^3}}{\rho^2} \quad (10.29)$$

where $\overline{(*)}$ denotes an average over the ring circumference.

Table 10.1 Radiation parameters^(a), energy loss and equilibrium quantities at the synchronous energy, E_s , in an isomagnetic ring

Critical photon energy, ϵ_c	keV	$\frac{3\hbar\gamma^3 c}{2\rho}$
Average photon energy, $\bar{\epsilon}$	keV	$\frac{8}{15\sqrt{3}} \epsilon_c$
rms energy spread, $\sqrt{(\epsilon - \bar{\epsilon})^2}$	keV	$\frac{\sqrt{211}}{15\sqrt{3}} \epsilon_c$
Energy loss, U_s	MeV / turn	$C_\gamma \frac{E_s^4}{\rho}$
Nb. of average photons	/turn/particle	$U_s/\bar{\epsilon}$
Longitudinal:		
equil. emittance, $\epsilon_{l,eq}$	$\mu\text{eV}\cdot\text{s}$	$\frac{\alpha E_s}{\Omega_s} \frac{C_q \gamma^2}{J_l \rho}$
rms energy spread, $\sigma_{\delta E/E}$		$\frac{1}{\sqrt{2}} \sigma_{\delta E/E} = \sqrt{\frac{C_q}{J_l \rho}} \gamma$
rms bunch length, σ_l	mm	$\frac{\alpha c}{\Omega_s} \sigma_{\delta E/E}$
Radial:		
equil. emittance, $\epsilon_{x,eq}$	nm	$= \frac{C_q \gamma^2}{J_x \rho} \mathcal{H}$
rms width, $\sigma_x(s)^{(b)}$	m	$\left(\beta_x(s) \epsilon_{x,eq} + D_x^2(s) \sigma_{\delta E/E}^2 \right)^{1/2}$
Damping times, $\tau_{x,y,l}$	ms	$\frac{T_{rev} E_s}{U_s J_{x,y,l}}$

(a) Units are, c: m/s; ρ : m; E_s : GeV

$$C_\gamma = \frac{4\pi}{3} \frac{r_0}{(m_0 c^2)^3} (= 8.846276 \cdot 10^{-5} \text{ m/GeV}^3 \text{ for electrons}).$$

$$C_q = \frac{55}{32\sqrt{3}} \frac{\hbar}{m_0 c} (= 3.8319386 \times 10^{-13} \text{ m for electrons}).$$

(b) With $\epsilon_{x,eq}, \beta(s)$ and dispersion $D_x(s)$ in meter.

2757 *Damping of accelerated motion*

2758 In an accelerator (a light source injector for instance), the RF voltage increases
 2759 during acceleration in order to compensate the increasing energy loss. To first order
 2760 in the invariant ε_u (with u standing for x or y) transverse damping in the presence
 2761 of acceleration satisfies [?]

$$\frac{d\varepsilon_u}{dt} = -\frac{2}{\tau_u(t)}\varepsilon_u + C_u(t) - \frac{1}{p} \frac{dp}{dt} \varepsilon_u, \text{ where } \tau_u^{-1} = J_u \frac{\bar{P}}{2E}, \begin{cases} C_x = \frac{\mathcal{H} \overline{N \langle \varepsilon^2 \rangle}}{E^2} \\ C_y = \frac{B_y}{2\gamma^2} \frac{\overline{N \langle \varepsilon^2 \rangle}}{E^2} \end{cases} \quad (10.30)$$

2762 Longitudinal damping satisfies

$$\frac{d(\widehat{\delta E})^2}{dt} = -\frac{2(\widehat{\delta E})^2}{\tau_l(t)} + (\dot{N} \langle \varepsilon^2 \rangle)(t) + \frac{(\widehat{\delta E})^2}{2E} \frac{dE_s}{dt} \quad \text{with } \tau_l^{-1} = J_l \frac{\bar{U}_s}{2E_s} \quad (10.31)$$

2763 ***** Figures ??, ?? display the evolution of horizontal and vertical emittance
 2764 with time, respectively

$$\bar{\varepsilon}_x(t) = \varepsilon_{x,0} \left(e^{t/|\tau_x|} - 1 \right), \quad \bar{\varepsilon}_y(t) = \varepsilon_{y,i} e^{-t/\tau_y} \quad (10.32)$$

2765 with $\varepsilon_{x,0}$ a constant and $\varepsilon_{y,i}$ an initial value.

2766 **10.2.6 Depolarizing resonances**

2767 By contrast with weak focusing optics where depolarizing resonances are weak
 2768 because horizontal field components are weak (Sect. 9.2.3), the use of strong fo-
 2769 cusing field gradients in the combined function magnets and/or focusing lenses of
 2770 strong focusing optics results in strong radial field components and therefore strong
 2771 depolarizing resonances.

2772 Spin precession and resonant spin motion in the magnetic components of a cyclic
 2773 accelerator have been introduced in Sects. 4.2.5, 5.2.5. The general conditions for
 2774 depolarizing resonance to occur have been introduced in Sect. 9.2.3. In a strong
 2775 focusing synchrotron they essentially result from the radial field components in the
 2776 focusing magnets and their strength is determined by the lattice optics, as follows.

2777 *Strength of imperfection resonances*

Imperfection, or integer, depolarizing resonances are driven by a non-vanishing vertical closed orbit $y_{co}(\theta)$ which causes spins to experience periodic radial fields in focusing magnets, dipoles in combined function lattices and quadrupoles in separated function lattices, namely,

$$B_x(\theta) = G y(\theta) = K(\theta) \times B_0 \rho_0 \times y_{co}(\theta)$$

with θ the orbital angle, $B_0 \rho_0$ the lattice rigidity and $y_{co}(\theta)$ the closed orbit excursion. Resonance occurs if the spin undergoes an integer number of precessions over a turn (it then undergoes 1-turn-periodic torques), so that spin tilts at field perturbations along the closed orbit add up coherently. Thus resonances occur at integer values

$$G\gamma_n = n$$

A Fourier development of these perturbative fields yields the strength of the $G\gamma_n$ harmonic [21, Sect. 2.3.5.1]

$$\epsilon_n^{\text{imp}} = (1 + G\gamma) \frac{R}{2\pi} \oint K(\theta) y_{co}(\theta) e^{-jG\gamma(\theta - \alpha)} e^{jn\theta} d\theta$$

2778 In the thin-lens approximation this simplifies into a series over the quadrupole fields,

$$\epsilon_n^{\text{imp}} = \frac{1 + G\gamma_n}{2\pi} \sum_{\text{Qpoles}} [\cos G\gamma_n \alpha_i + \sin G\gamma_n \alpha_i] (KL)_i y_{co}(\theta_i) \quad (10.33)$$

2779 with θ_i the quadrupole location, $(KL)_i$ the integrated strength (slice the dipoles as
2780 necessary in an AG lattice for this series to converge) and α_i the cumulated orbit
2781 deviation.

2782 Orbit harmonics near the betatron tune ($n = G\gamma_n \approx \nu_y$) excite strong resonances.
2783 Imperfection resonance strength is further amplified in P-superperiodic rings, with
2784 m-cell superperiods, if the betatron tune $\nu_y \approx \text{integer} \times m \times P$ [22, Chap.3-I].

2785 *Strength of imperfection resonances*

2786 Intrinsic depolarizing resonances are driven by betatron motion, which causes spins
2787 to experience strong radial field components in quadrupoles, namely

$$B_x(\theta) = G y(\theta) = K(\theta) \times B_0 \rho_0 \times y_\beta(\theta) \quad (10.34)$$

The effect of resonances on spin depends upon betatron amplitude and phase, their effect on beam polarization depends on beam emittance. Longitudinal fields from dipole ends are usually weak by comparison and ignored. The location of intrinsic resonances depends on betatron tune, it is given in an M-periodic structure by

$$G\gamma_n = nM \pm \nu_y$$

2788 **10.3 Exercises**

2789 In complement to the present exercises, an extensive tutorial on depolarizing res-
 2790 onances in a strong focusing synchrotron, considering proton, helion, or electron
 2791 beams, using the lattice of the AGS Booster at BNL, can be found in Ref. [21],
 2792 Chap. 14, "Spin Dynamics Tutorial: Numerical Simulations". The simulaitions in-
 2793 clude tune-jump quadrupoles, solenoid, snakes, electron beam polaization life time
 2794 and spin rotators.

2795 **10.1 Construct SATURNE II synchrotron. Spin Dynamics With Snakes**

2796 Solution: page 361

2797 Over the years 1978-1997 the 3 GeV synchrotron SATURNE II at Saclay
 2798 (Fig. 10.7) delivered ion beams up to 1.1 GeV/nucleon, including polarized proton,
 2799 deuteron and ${}^6\text{Li}$ beams, for intermediate energy nuclear physics research, including
 2800 meson production [17, 18]. The separated function synchrotron was designed *ab*
 2801 *initio* for the acceleration of polarized beams [20], and the first strong focusing syn-
 2802 chrotron to do so - ZGS, first to accelerate polarized beams, protons and deuterons,
 2803 was a weak focusing synchrotron (see Chap. 9).

2804 SATURNE II is a FODO lattice with missing dipole. Its parameters are given in
 2805 Tab. 10.2.

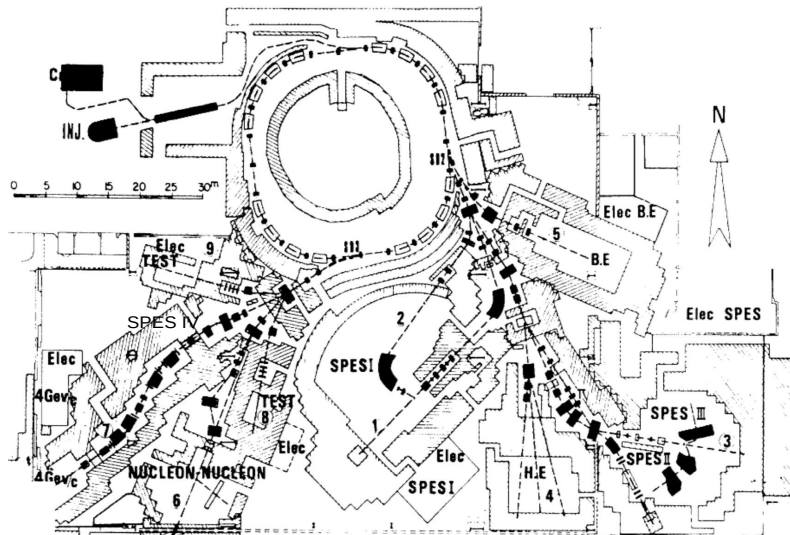


Fig. 10.7 SATURNE II synchrotron and its experimental areas [23], including mass spectrometers SPES I to SPES IV, a typical 1960-80s nuclear physics accelerator facility. Polarized ion sources are on the top left, followed by a 20 MeV linac

(a) Simulate the main dipole using BEND, include fringe fields assuming $\lambda = 8$ cm extent and the following Enge coefficient values (Eq. 15.13, Sect. 15.2.6):

Table 10.2 Parameters of SATURNE II separated function FODO lattice. ρ_0 denotes the reference bending radius in the main dipole; the reference orbit, wave numbers, etc., are taken along that radius

Orbit length, C	m	105.5556
Average radius, $R = C/2\pi$	m	16.8
Length of long straight section	m	
Wave numbers, $\nu_x; \nu_y$		3.64; 3.60
Chromaticities, $\xi_x; \xi_y$		negative, a few units
Momentum compaction α		0.015
Injection energy (proton)	MeV	20
Top energy	GeV	3
\dot{B}	T/s	4.2
Synchronous energy gain	keV/turn	1.160
RF harmonic		2
Dipole:		
- bend angle, α	deg	$\pi/8$
- magnetic length, $\rho\alpha$	m	2.489
- magnetic radius, ρ	m	6.3381
- wedge angle, ε	deg	2.45
Quadrupole:		
- gradient	T/m	0.5 - 10.56
- magnetic length F/D	m	0.46723 / 0.486273

$$C_0 = 0.2401, C_1 = 1.8639, C_2 = -0.5572, C_3 = 0.3904, C_4 = C_5 = 0$$

2806 Produce a graph of the field across the dipole along the reference orbit, in the median
2807 plane and at 5 cm vertical distance. Produce the transport matrix, check against theory.
2808 Compare with the matrix of the hard edge model.

2809 Simulate the F and D quadrupoles, using respectively QUADRUPOLE and MUL-
2810 TIPOL. Compare matrices with theory.

2811 Construct the cell. Produce machine parameters (tunes, chromacities), check
2812 against data, Tab. 10.2.

2813 Construct the 4-cell ring. Produce a graph of the optical functions.

2814 (b) Accelerate a bunch with Gaussian densities comprised of a few tens of particles
2815 (it can be defined using MCOBJET), from injection to top energy; use harmonic 3
2816 RF frequency, and (unrealistic, for a reduced number of turns) peak RF voltage
2817 $\hat{V} = 1$ MV.

2818 Produce a graph of the three phase spaces. Check the transverse betatron damping.

2819 (c) Simulate multiturn injection in the ring. Take the injection point at the center
2820 of a long straight section.

2821 (d) Simulate resonant extraction from the ring, on $\nu_x = 11/3$. Take the extraction
2822 point at the center of a long straight section.

2823 10.2 Depolarizing Resonances In SATURNE II

2824 The input data file to simulate the ring is given in Tab. 17.73, an outcome of
2825 exercise 10.1.

2826 (a) Calculate the strength of the intrinsic depolarizing resonances (systematic and
2827 non-systematic) over 0.5-3 GeV, using Eq. ??.

2828 (b) $G_{\gamma}=7-\nu_y$ was found to be a potentially harmful depolarizing resonance
2829 - unexpectedly as this is not a systematic resonance. Produce a crossing of that
2830 resonance, for a 100-particle bunch. Get its strength from this simulation, compare
2831 with (a).

2832 (c) Multiple resonance xing - ref to Phys. Rev. article ***

2833 **10.3 Cornell electron RCS. Radiative Energy Loss**

2834 Short intro energy loss by synchrotron radiation [24]

2835 Tab.: RCS parameter list

2836 (a) Cornell RCS parameters are given in Tab. ???. Construct the ring, produce its
2837 optical parameters. Produce a graph of the optical functions.

2838 (b) Raytrace a few tens of particles over 3000 turns in Cornell RCS, from ***
2839 to *** GeV. Assume emittances $\epsilon_{x,y}$, Gaussian densities, initial *rms*
2840 $\delta p/p = 10^{-4}$. Produce a graph of the three phase spaces. produce graphs of horizontal
2841 and vertical transverse excursions versus turn number.

2842 (c) Re-do (b) with synchrotron radiation energy loss.

2843 (d) Produce the average beam polarization obtained in (c).

2844 (c) Multiple resonance crossing.

References

- 2846 1. Christofilos, Nicholas: Focussing system for ions and electrons. US Patent Office Application
2847 filed March 10, 1950, Serial No. 148,920.
2848 <https://patentimages.storage.googleapis.com/fa/bb/52/0ce28e28b492a6/US2736799.pdf>
- 2849 2. Courant, Ernest D., Livingston, M. Stanley, and Snyder, Hartland S.: The Strong-Focusing
2850 Synchrotron - A New High Energy Accelerator. Phys. Rev. 88, 1190 - December 1952
- 2851 3. Courant, E. D., and Snyder, H. S.: Theory of the Alternating-Gradient Synchrotron. Annals
2852 of Physics, No. 3 (1958), 1-48
- 2853 4. Credit: Brookhaven National Laboratory.
2854 <https://www.flickr.com/photos/brookhavenlab/8495311598/in/album-72157611796003039/>
- 2855 5. I. Agapov, et al.: Future Circular Lepton Collider FCC-ee: Overview and Status. Submitted
2856 on 15 Mar 2022; arXiv:2203.08310 [physics.acc-ph].
2857 <https://doi.org/10.48550/arXiv.2203.08310>
- 2858 6. Méot, F., et al.: Progress on the optics modeling of BMII ion rapid-cycling medical
2859 synchrotron at BNL. THPMP050, 10th Int. Particle Accelerator Conf. IPAC2019, Melbourne,
2860 Australia. <https://accelconf.web.cern.ch/ipac2019/papers/thpmp050.pdf>
2861 Copyrights under license CC-BY-3.0, <https://creativecommons.org/licenses/by/3.0/>; no change
2862 to the material
- 2863 7. Nishimori, N.: A new compact 3 GeV light source in Japan. 13th Int. Particle Acc. Conf.
2864 IPAC2022, Bangkok, Thailand.
2865 <https://accelconf.web.cern.ch/ipac2022/papers/thixsp1.pdf>
- 2866 8. Radial Focusing in the Linear Accelerator. Phys. Rev. Vol. 88, Num. 5, Dec. 1, 1952
- 2867 9. Benabderrahmane, C.: Status of the ESRF-EBS magnets. WEPMK009, 9th International
2868 Particle Accelerator Conference, IPAC2018, Vancouver, BC, Canada.
2869 <https://accelconf.web.cern.ch/ipac2018/papers/wepmk009.pdf>
- 2870 10. Credit: Lawrence Berkeley National Laboratory. The Regents of the University of California,
2871 Lawrence Berkeley National Laboratory."
- 2872 11. Jackson, G., Editor: Fermilab recycler ring technical design report. Rev. 1.1. FERMILAB-
2873 TM-1981 (July 1996).
2874 <http://inspirehep.net/record/424541/files/fermilab-tm-1981.PDF>
- 2875 12. Méot, F.: On the Effects of Fringe Fields in the Recycler Ring. FERMILAB-TM-2016
2876 (Aug. 1997).
2877 <http://inspirehep.net/record/448603/files/fermilab-tm-2016.PDF>
- 2878 13. Ahrens, L., et al.: Development of a stepwise ray-tracing based on-line model at the AGS.
2879 WEP141, Proceedings of 2011 Particle Accelerator Conference, New York, NY, USA.
2880 <https://accelconf.web.cern.ch/PAC2011/papers/wep141.pdf>
- 2881 14. Leleux, G.: Compléments sur la Physique des Accélérateurs. DEA "Physique et Technologie
2882 des Grands Instruments", Université Paris VI. Rapport interne LNS//86-101, CEA Saclay
2883 (1986)
- 2884 15. F. Méot, et al.: Beam dynamics validation of the Halbach Technology FFAG Cell for Cornell-
2885 BNL Energy Recovery Linac. Nuclear Inst. and Methods in Physics Research, A 896 (2018)
2886 60-67
- 2887 16. Leleux, G.: Accélérateurs Circulaires. INSTN lectures, internal report CEA Saclay (1978),
2888 unpublished
- 2889 17. The 20 Years of the Synchrotron SATURNE-2. In: Proceedings of the Colloquium, Paris,
2890 France, 04 - 05 May 1998, A. Boudard and P.-A. Chamouard Editors. Edited By CEA -
2891 Laboratoire National SATURNE & CEN Saclay, France.
2892 <https://doi.org/10.1142/3965>
- 2893 18. Plus d'anneaux autour de SATURNE (pp. 33-34) Published in: Courrier CERN Volume 39,
2894 N° 2, Mars 1999.
2895 <https://cds.cern.ch/record/1740121>
- 2896 19. Hofmann, A.: The Physics of Synchrotron Radiation. Cambridge Monographs on Particle
2897 Physics, Nuclear Physics and Cosmology (20), Cambridge University Press (2004)

- 2898 20. E. Grorud, J.L. Laclare and G. Leleux: Crossing of Depolarization Resonances in Strongly
2899 Modulated Structures. IEEE Transactionson NuclearScience, Vol. NS-26,NO. 3, June 1979.
2900 https://accelconf.web.cern.ch/p79/PDF/PAC1979_3209.PDF
- 2901 21. Méot, F.: Polarized Beam Dynamics and Instrumentation in Particle Accelerators, USPAS
2902 Summer 2021 Spin Class Lectures, Springer Nature, Open Access (2023).
2903 <https://link.springer.com/book/10.1007/978-3-031-16715-7>
- 2904 22. Lee, S.Y: Spin Dynamics and Snakes in Synchrotrons. World Scientific (1997)
- 2905 23. Aknin, J.P., et al.: Status report on rejuvenating SATURNE and future aspects. PAC 1979
2906 Conference. IEEE Tans. Nucl. Sci., Vol. NS 26, No. 3, June 1979.
2907 https://accelconf.web.cern.ch/p79/PDF/PAC1979_3138.PDF
- 2908 Figure 10.7: Copyrights under license CC-BY-3.0,
2909 <https://creativecommons.org/licenses/by/3.0>; no change to the material; “SPES IV”
2910 has been added on the picture
- 2911 24. D. L. Rubin, et al.: Upgrade of the Cornell electron storage ring as a synchrotron light source.
2912 WEPOB36, Proceedings of NAPAC2016, Chicago, IL, USA.
2913 <https://accelconf.web.cern.ch/napac2016/papers/wepob36.pdf>